Generating and Dimerizing the Transient 16-Electron Phosphinidene Complex [Cp*Ir=PAr]: A Theoretical and Experimental Study

Arjan T. Termaten,[a] Tom Nijbacker,[a] Andreas W. Ehlers,[a] Marius Schakel,[a] Martin Lutz,[b] Anthony L. Spek,[b] Michael L. McKee,[c] and Koop Lammertsma*[a]

Abstract: The properties of the 16-electron phosphinidene complex [CpRIr=PR] were investigated experimentally and theoretically. Density functional theory calculations show a preferred bent geometry for the model complex [CpIr=PH], in contrast to the linear structure of [CpIr=NH]. Dimerization to give [{CpIr=PH}$_2$] and ligand addition to afford [Cp(L)Ir=PH] (L = PH_3, CO) were calculated to give compounds that were energetically highly favorable, but which differed from the related imido complexes. Transient 16-electron phosphinidene complex [Cp*Ir=PAr] could not be detected experimentally. Dehydrohalogenation of [Cp*IrCl_2(PH_2Ar)] in CH_2Cl_2 at low temperatures resulted in the novel fused-ring systems **17** (Ar = Mes*) and **20** (Ar = Mes), with dimeric [{Cp*Ir=PAr}$_2$] being the likely intermediate. Intramolecular C–H bond activation induced by steric factors is considered to be the driving force for the irreversible formation of **17** and **20**. ONIOM calculations suggest this arises because of the large steric congestion in [{Cp*Ir=PAr}$_2$], which forces it toward a more reactive planar structure that is apt to rearrange.

Keywords: density functional calculations · iridium · N ligands · P ligands

Introduction

In the past twenty years transition metal phosphinidene complexes, [L_nM=PR], have evolved as valuable reagents in organophosphorus chemistry.[1–3] One of their most intriguing features is their ability to mimic carbene complexes, as demonstrated by the availability of both electrophilic (Fischer-type) and nucleophilic (Schrock-type) phosphinidene complexes.[3] The vertical N–P relationship in the Periodic Table is not prevalent for low-coordinate species because of the higher electronegativity of nitrogen with respect to phosphorus.[3a] Although comparable nucleophilic phosphinidene and imido complexes have been prepared, their properties differ.[4–7] This is a theme we explore in more detail in the present study.

Recently, we reported on novel iridium phosphinidene complexes generated by dehydrohalogenation of primary phosphine complexes **1** (Scheme 1). The linear phosphinidene complexes **2** eluded detection, but the highly stable bent phosphinidene complexes [Cp*(L)Ir=PAr] (**3**) were obtained in the presence of stabilizing ligands (L = PR_3, AsR_3, dppe, RN≡C, CO; Ar = Mes*, Is, Mes).[8] Similar complexes could be prepared for the other members of the Group 9 transition metal triad (Co, Rh). All these complexes show a surprisingly low reactivity.[9]

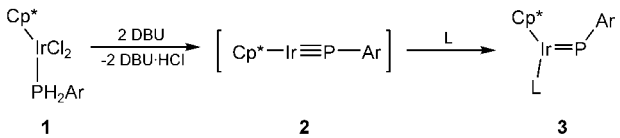

Scheme 1.

Of course, in the absence of a stabilizing ligand a much higher reactivity is expected. This encouraged us to explore in more detail the properties of **2** in comparison to that of its imido analogue. We chose to focus on iridium as the transition metal since its imido, oxo, and carbene complexes are

[a] Dr. A. T. Termaten, T. Nijbacker, Dr. A. W. Ehlers, Dr. M. Schakel, Prof. Dr. K. Lammertsma
Department of Chemistry, Faculty of Sciences
Vrije Universiteit
De Boelelaan 1083, 1081 HV, Amsterdam (The Netherlands)
Fax: (+31) 20-444-7488
E-mail: lammert@few.vu.nl

[b] Dr. M. Lutz, Prof. Dr. A. L. Spek
Bijvoet Center for Biomolecular Research
Department of Crystal and Structural Chemistry
Utrecht University
Padualaan 8, 3584 CH, Utrecht (The Netherlands)

[c] Prof. Dr. M. L. McKee
Department of Chemistry, Auburn University
Auburn, Alabama 36849 (USA)

Supporting information for this article is available on the WWW under http://www.chemeurj.org/ or from the author.

 DOI: 10.1002/chem.200400080

known experimentally, whereas the Co and Rh congeners are more elusive.

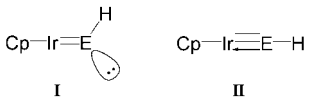

I II

Results and Discussion

We begin with a density functional theory (DFT) analysis on unsubstituted model complexes to address the viability and reactivity of **2** in comparison to that of the well-explored imido analogue [Cp*Ir≡NR].[10] Next, we describe low-temperature experiments on the dehydrohalogenation of **1**, and the isolation and characterization of novel dimerization products. The large influence that steric congestion has on the fate of **2** and its dimer will be illustrated with the assistance of theoretical calculations.

Theoretical evaluation of [CpIrPH]: Before evaluating their susceptibility to ligation and dimerization, the structural and electronic properties of [CpIrEH] (E = N, P) will be analyzed.

Structural and electronic properties of [CpIrEH] (E = P, N): Two canonical structures can be depicted, a bent 16-electron geometry (**I**) with an Ir=E double bond and a linear 18-electron structure (**II**) with an Ir≡E triple bond.

Most imido complexes prefer a linear geometry (**II**), an issue that has been addressed theoretically.[11,12] In contrast, phosphinidene complexes are typically bent (M=P–R 109–116°).[1b,3] In fact, only two linear phosphinidene complexes are known, namely [{$(Me_3SiNCH_2CH_2)_3N$}Ta≡PCy][4a] and [$(CO)(PPh_2Me)_2Cl_2W$≡PMes*],[5a] both of which are stabilized by bulky ligands and substituents. The linear complexes have electron deficient metal centers with the phosphinidene acting as a four-electron donor. The isoelectronic zirconocene complexes [$Cp_2(PMe_3)$Zr=PMes*] (Zr–P–Mes* 116.1°)[6] and [Cp_2(thf)Zr=N*t*Bu] (Zr–N–*t*Bu 174.4°)[7] underscore the differences between the phosphinidene and imido complexes.

BP86/TZP optimized geometries of imido and phosphinidene complexes [CpIr≡EH] are depicted in Figure 1. The

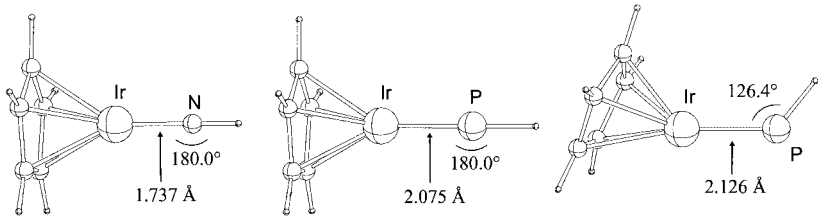

4 **5** **6**

Figure 1. BP86/TZP geometries for [Cp–Ir≡N–H] (**4**, C_{5v}), [Cp–Ir≡P–H] (**5**, C_{5v}), and [Cp–Ir=P–H] (**6**, C_s).

1.737 Å Ir≡N bond for linear imido complex **4** (C_{5v}) compares well with the experimental values reported for [Cp*Ir≡NR] (1.712–1.750 Å).[10] The 2.075 Å Ir≡P bond for linear compound **5** (C_{5v}) is shorter than the 2.126 Å Ir=P bond for bent **6**, the latter resembling those reported for bent phosphinidene complexes [Cp*(L)Ir=PMes*] (2.1783(8)–2.2121(5) Å).[8] In contrast to the imido complex, **6** (∢Ir–P–H 126.4°) is a minimum whereas **5** is not (with a degenerate imaginary frequency of $-79.8\,cm^{-1}$), but as the potential energy surface is very flat for this compound (Figure 2), the inversion barrier is only 1.1 kcal mol^{-1}.

Energy decomposition of the metal–phosphorus bond into orbital interaction (ΔE^{oi}), electrostatic interaction (ΔE^{o}),

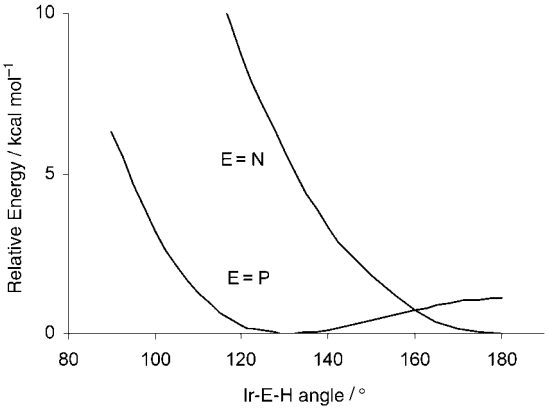

Figure 2. Energy plot for varying the Ir–E–H angle in [CpIr=EH].

Abstract in Dutch: *De eigenschappen van het 16e fosfinideen complex RIr=PR worden theoretisch en experimenteel onderzocht. DFT-berekeningen tonen aan dat het model-complex [CpIr=PH] in tegenstelling tot de lineaire structuur van [CpIr≡NH] een gebogen geometrie prefereert. De berekeningen laten zien dat zowel dimerisatie naar [{CpIr=PH}$_2$] als ook ligand additie tot [Cp(L)Ir=PH] (L = PH_3, CO) beide energetisch zeer voordelig zijn, wat sterk verschilt van het verwante imido complex. Het kortlevende 16e fosfinideen complex [Cp*Ir=PAr] kon experimenteel niet waargenomen worden. In plaats hiervan leidde dehydrohalogenering van [Cp*IrCl$_2$(PH$_2$Ar)] in CH_2Cl_2 bij lage temperaturen tot de nieuwe gefuseerde ring systemen **17** (Ar = Mes*) en **20** (Ar = Mes), waarschijnlijk met het dimere [{Cp*Ir=PAr}$_2$] als intermedair. Intramoleculaire C–H bond activering geïnduceerd door sterische factoren wordt als de drijvende kracht achter de irreversibele vorming van **17** en **20** gezien. ONIOM berekeningen suggereren dat op grond van de grote sterische hinder [{Cp*Ir=PAr}$_2$] in een meer planaire en reaktievere vorm gedwongen wordt die gemakkelijk omlegt.*

and preparation energy (ΔE^{prep}) terms illustrates the different features of **4**, **5**, and **6** (Table 1). In the triply bonded linear complexes the degenerate π bonds result from interaction of the p_x and p_y singly occupied orbitals (SOMO) of the EH fragment with the d_{xz} and d_{yz} ones of IrCp,[13] while the σ bond arises from an interaction between the p_z lone pair of EH with the d_{z^2} orbital of IrCp. As the SOMO energy of the NH fragment (−8.00 eV) in the equilibrium geometry is much lower than that of PH (−6.20 eV), a greater amount of charge is transferred from the CpIr fragment upon bond formation in **4** than in **5**; this is also evident from the calculated Hirshfeld charges for N (−0.23) and P (−0.07).[14] The higher bond dissociation energy (BDE) for the Ir≡N bond (150.0 kcal mol^{-1}) in comparison to the Ir≡P bond (110.0 kcal mol^{-1}) is due to the large difference in the total orbital interaction energy ΔE^{oi} (**4** −235.6, **5** −153.4 kcal mol^{-1}), as it is only partly offset by the higher steric interaction ($\Delta E°$) for the tighter complex. The relative contribution of σ bonds (ΔE_σ) to ΔE^{oi} is similar for both complexes (~28%).

Table 1. Bond energy evaluation (kcal mol^{-1})[a] for the Ir≡E bonds in **4**, **5**, and the Ir=P bond in **6**.

Complex	ΔE_σ	ΔE_π	ΔE^{oi}	$\Delta E°$	ΔE^{tot}	BDE
[CpIr≡NH] (**4**)	−64.6	−171.2	−235.6	+81.2	−154.4	+150.0
[CpIr≡PH] (**5**)	−44.9	−107.1	−153.4	+41.0	−112.4	+110.0
[CpIr=PH] (**6**)	−114.9	−49.9	−164.8	+54.7	−110.1	+111.1

[a] For definitions see the Computational Section.

When the Ir–P–H moiety is bent, the π degeneracy ceases to exist (P $sp \rightarrow sp^2$) and a lone pair is found on phosphorus; this enhances the ΔE_σ contribution (−114.9 kcal mol^{-1}) to ΔE^{oi} at the expense of ΔE_π (−49.9 kcal mol^{-1}), while the other energy terms exhibit only minor changes. The bonding features of the Ir=P bond in **6** resemble that of related bent 18-electron complexes like [Cp(PH$_3$)Ir=PH] (ΔE_σ −112.3, ΔE_π −39.1 kcal mol^{-1}).[15]

Bent phosphinidene complex **6** has a low-lying LUMO (−3.22, **4** −2.10, **5** −2.61 eV) with large coefficients at the unprotected side of the Ir=P bond (Figure 3a). As its character differs from the degenerate, higher-lying π* LUMO of the linear imido complex **4** (Figure 3b), a different reactivity is expected, one which we explored for ligation and dimerization.

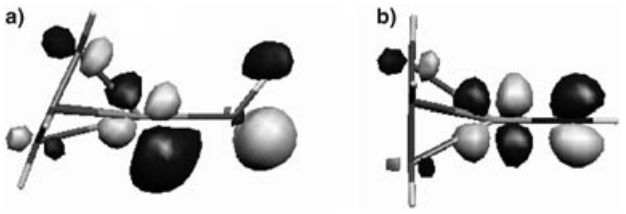

Figure 3. LUMO of a) bent [CpIr=PH] (**6**), and b) linear [CpIr≡NH] (**4**).

Ligand addition: The different electronic properties of **6** and **4** are evident from their ligation with, for example, CO and PH$_3$, the adducts of which are depicted in Figure 4. Ligation to give phosphinidene complex [Cp(L)Ir=PH] occurs without barrier and with high exothermicity (**7** −59.6 kcal mol^{-1} (CO), **8** −42.2 kcal mol^{-1} (PH$_3$)). This process concurs with the reported synthesis of the stable bent phosphinidene adducts [Cp*(L)Ir=PMes*], which are shown in Scheme 1.[8] Clearly, the interaction at the metal center of the LUMO in **6** is very favorable for donor ligands. However, in **4** this picture is different. Upon addition of CO and PH$_3$ we found two transition state structures that exhibited barriers of 5.8 and 7.8 kcal mol^{-1}, respectively, and ligand addition to subsequently give imido complexes [Cp(CO)Ir=NH] (**9**) and [Cp(PH$_3$)Ir=NH] (**10**) proceeded with much less exothermicity (**9** −22.0, **10** −8.7 kcal mol^{-1}). It is not surprising then that Bergman et al.[10] found the more congested [Cp*Ir≡N*t*Bu] to be unreactive toward phosphines. With the smaller CO molecule they observed the formation of isocyanate complex [Cp*(CO)IrC(O)N(*t*Bu)],[16] possibly by initial metal CO ligation to give [Cp*(CO)Ir≡N*t*Bu] (**9**) followed by intramolecular attack of the imido moiety at the CO ligand and subsequent addition of a second CO molecule at the metal center. The potential energy surface for the model system is given in Figure 5. It shows the cyclization of [Cp(CO)Ir≡NH] to be isothermic with a modest barrier (17.5 kcal mol^{-1}), while addition of a second CO molecule is highly exothermic (−44.0 kcal mol^{-1}). The nucleophilicity of the imido unit in **9** is supported by the large Hirshfeld charge at nitrogen (−0.27). In contrast, the phosphorus center in **7** (−0.02) does not exhibit nucleophilicity, and in concurrence with experiments is not prone to ring closure.[8]

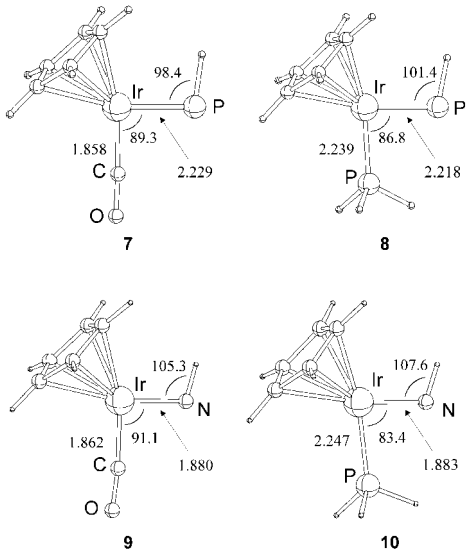

Figure 4. BP86/TZP optimized structures for the CO and PH$_3$ adducts of [CpIr=PH] and [CpIr≡NH].

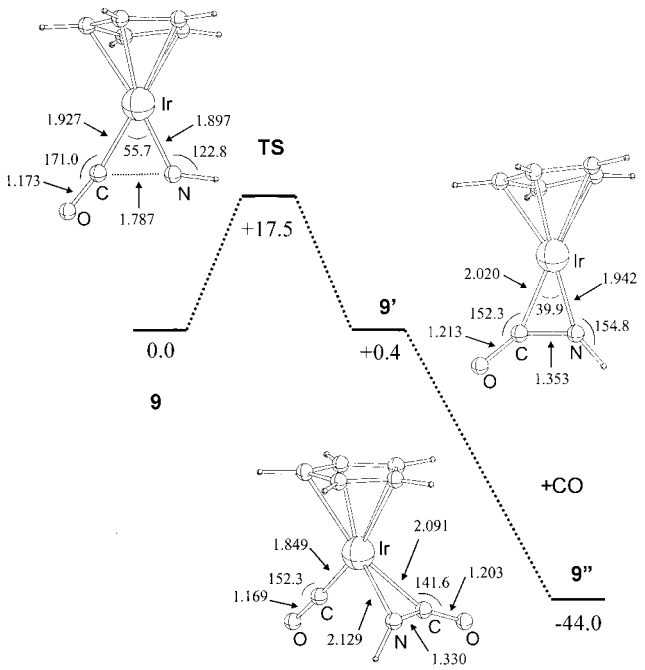

Figure 5. Energy profile (BP86/TZP) for the reaction of CO with CpIr≡NH.

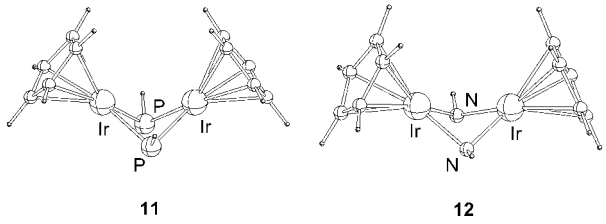

Figure 6. BP86/TZP optimized geometries of [{CpIrPH}$_2$] (**11**, C_s) and [{CpIrNH}$_2$] (**12**, C_s).

Table 2. BP86/TZP bond lengths [Å], angles [°], and torsion angles [°] for the [{CpIrEH}$_2$] dimers.[a]

	[{CpIrPH}$_2$] (**11**)	[{CpIrNH}$_2$] (**12**)
Ir–E	2.308 (2.325)	1.987
Ir–Ir′	2.874 (2.894)	2.721
Cp–Ir	1.891 (1.894)	1.865
Cp-Ir-E	140.6 (140.9)	142.7
Ir-Ir′-E	51.6 (51.5)	46.8
E-Ir-E′	78.8 (78.4)	74.2
Ir-E-E′-Ir′	107.3 (106.9)	118.3

[a] Values in parenthesis are at the B3LYP/6-31G^{++} level with LANL2DZ for Ir.

Dimerization: In the absence of a stabilizing ligand dimerization of [CpIr=PR] is a viable option. Although to our knowledge such dimers have not been reported in the literature, stable [{Cp*IrNR}$_2$] complexes have been synthesized by thermal and water-catalyzed dimerization of [Cp*Ir≡NR].[17] For parent **4** this process is exothermic (−39.0 kcal mol^{-1}), while for phosphorus analogue **6** it is tremendously exothermic (−96.4 kcal mol^{-1}). Hence, the possibility of identifying a 16-electron [CpIr=PR] complex must be considered small. The DFT optimized structures of [{CpIrPH}$_2$] (**11**) and [{CpIrNH}$_2$] (**12**) are depicted in Figure 6, while selected bond lengths and angles are collected in Table 2. The structure of **12**, which agrees well with the experimental one determined for [{Cp*IrNPh}$_2$],[17] has elongated Ir–N bonds (1.987 versus 1.737 Å for **4**), a short Ir–Ir distance (2.721 Å), and a puckered Ir_2N_2 ring (∢Ir-N-N′-Ir′ 118.3°) that has pyramidal imido centers (sum of angles 326°). The lower stability of the planar Ir_2N_2 isomer ($\Delta E = 15.8$ kcal mol^{-1}) has been attributed to second-order Jahn–Teller distortion.[17b] Likewise, [{CpIrPH}$_2$] favors the even more puckered structure **11** (Ir-P-P′-Ir′ 107.3°) by 12.5 kcal mol^{-1} with pyramidal phosphorus centers (sum of angles 299°), long Ir–P bonds (2.308 Å), and an Ir–Ir distance of 2.874 Å. This encouraged us to explore in more detail the potential dimerization of **2**.

Generating and dimerizing [Cp*Ir=PAr]: To identify [Cp*Ir=PAr] or its primary adducts, the dehydrohalogenation of phosphine complex **1** with the strong phosphazene base *tert*-butylimino-tri(pyrrolidino)phosphorane (BTPP; p$K_B \approx 26$) was monitored by ^{31}P NMR spectroscopy. Addition of two equivalents of BTPP to **1a** at room temperature gave a purple-colored dichloromethane solution in which only the known [Cp*(PH$_2$Mes*)Ir=PMes*] (**13**; Mes* = 2,4,6-tri-*tert*-butylphenyl)[8] and [{Cp*IrCl$_2$}$_2$] (**14**)[18] were identified as the major products (Scheme 2). This suggests that [Cp*Ir=PMes*], which abstracts PH$_2$Mes* from its precursor, is an intermediate, and implies that the second dehydrohalogenation is faster than the first. However, upon using only one equivalent of BTPP for the HCl abstraction at −70 °C, neither **13** nor its precursor [Cp*(Cl)Ir=P(H)Mes*] were detected. Instead, based on the ^{31}P NMR doublet of doublets at $\delta = 386$ ($^3J_{P,H} = 36$ Hz) and −126 ppm ($^1J_{P,H} = 446$ Hz) in which the $^2J_{P,P}$ coupling constants were identical (43 Hz), the major product was identified as **15**.

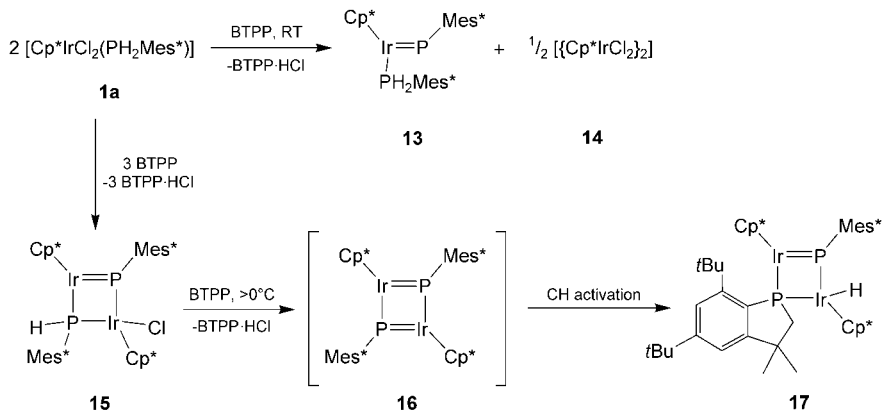

Scheme 2.

This asymmetric dimer may be formed by reaction of phosphinidene [Cp*Ir=PMes*] with phosphide precursor [Cp*(Cl)Ir=P(H)Mes*], and does indeed mean that the second dehydrohalogenation is faster than the first. More importantly, it also indicates that [Cp*Ir=PMes*] is a highly reactive intermediate. Formation of **15** is complete with 1.5 equivalents of BTPP. To obtain dimer **16** another HCl molecule must be abstracted; this was attempted with the addition of 0.5 equivalents of BTPP and slow warming to 0 °C. While this gave an air-sensitive, high-melting (>320 °C), dark red solid that crystallized quantitatively from the reaction mixture, its characterization proved to be more difficult.

An X-ray crystal structure confirmed the dimeric nature of the compound isolated (Figure 7). Unfortunately, it also showed disorder in the *ortho tert*-butyl groups. As a consequence, the geometry of the central Ir_2P_2 ring was not reliable, and crystallographic discrimination between a symmetrical dimer [{Cp*IrPMes*}$_2$] (**16**, planar or puckered) and an asymmetric system such as **17** was hampered despite the large internal differences between the four Ir–P distances in the crystal structure (2.167(4)–2.300(8) Å). However, the structure could be assigned to **17** with the aid of ^{31}P and ^{1}H NMR spectra recorded in CD_2Cl_2 at 50 °C.[19] These showed two $\delta(^{31}P)$ resonances at +183 ($^{2}J_{P,H}$ = 34 Hz) and −176 ppm ($^{2}J_{P,H}$ = 25 Hz) with a large $^{2}J_{P,P}$ coupling constant of 198 Hz, and $\delta(^{1}H)$ resonances for an Ir–H fragment (−14.8 ppm), a CH_2 group (3.25 ppm), and an abundance of different CH_3 groups. The formation of **17** likely proceeds via intermediate **16** even though it could not be detected during the reaction. Carbon–hydrogen bond activation of a *tert*-butyl group through an agostic interaction with a nearby iridium center may induce the hydrogen transfer and 'phosphinidene insertion'.

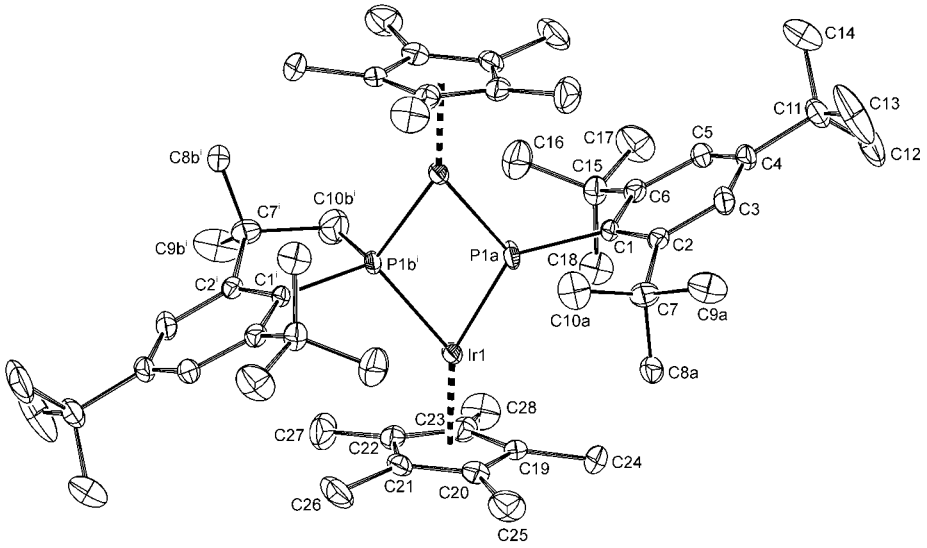

Figure 7. Structure of **17** (displacement ellipsoid plot; 50% probability level). Hydrogen atoms are omitted for clarity. The molecule is located on a crystallographic inversion center and was refined with a disorder model. The disorder component with the phosphinidene ligand is drawn on the right-hand side. The disorder component with the iridium hydride and the cyclic phosphide ligand is drawn on the left-hand side. The position of the hydride could not be determined. Symmetry operation: $1-x, 1-y, 1-z$.

To further explore the [{Ir_2P_2}$_2$] dimer, we sought to reduce its steric congestion by replacing the *tert*-butyl groups on phosphorus with methyl groups (i.e. Mes = 2,4,6-trimethylphenyl rather than Mes*). This would also have the further effect of eliminating the formation of phosphinidenes like **17**.[20] However, dehydrohalogenation of [Cp*$IrCl_2$(PH_2Mes)] (**1b**) with one equivalent of BTTP in CD_2Cl_2 at −80 °C (Scheme 3) gave two symmetrical and one asymmetrical isomer of [Cp*(Cl)Ir=P(H)Mes] dimer **18** in a ratio of 1:2:10, as characterized by their respective ^{31}P NMR resonances at δ = −208 ($^{1}J_{P,H}$ = 359 Hz), −189 ($^{1}J_{P,H}$ = 354 Hz), −147 ($^{1}J_{P,H}$ = 351 and $^{2}J_{P,P}$ = 166 Hz), and −202 ppm ($^{1}J_{P,H}$ = 367 and $^{2}J_{P,P}$ = 166 Hz). Evidently, less crowded [Cp*(Cl)Ir=P(H)Mes] dimerizes rather than undergoing elimination of HCl. Upon addition of a second equivalent of BTPP at room temperature, and based upon the single $\delta(^{31}P)$ resonance at −170 ppm ($^{1}J_{P,H}$ = 308 Hz) as well as ^{1}H NMR resonances for PH, CH_2, and two non-equivalent CH_3 groups, **18** was converted into phosphametallacycle **20** (68%). An X-ray crystal structure determination confirmed the centrosymmetric structure of **20** (Figure 8, Table 3) in which the [IrP]$_2$ ring is planar and the phosphorus centers have a tetrahedral geometry.

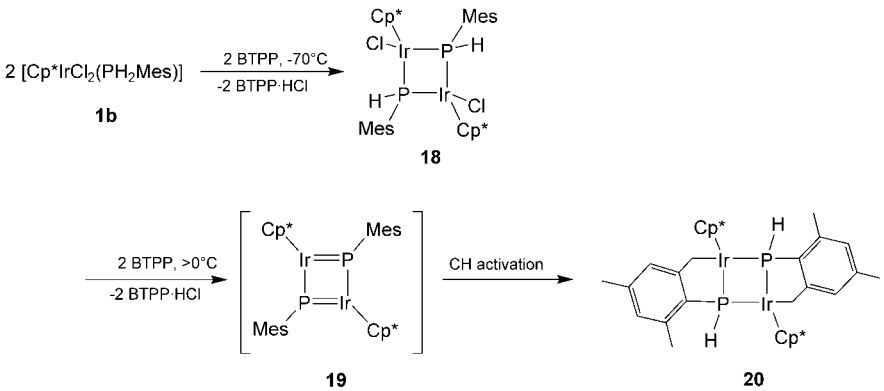

Scheme 3.

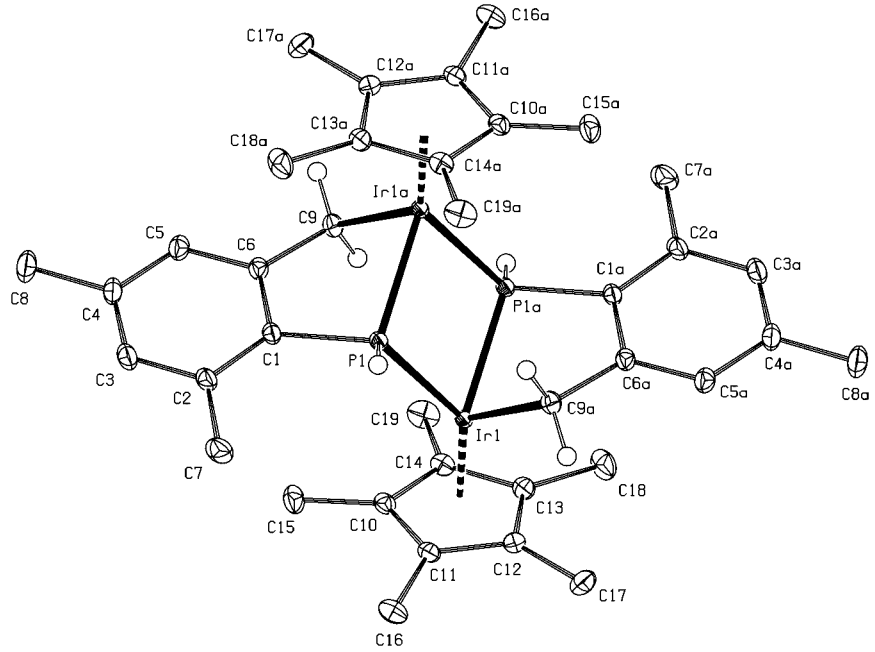

Figure 8. Structure of **20** (displacement ellipsoid plot; 50% probability level). For the purpose of clarity only the hydrogens on phosphorus and the CH_2 groups are depicted. Symmetry operation: $1-x, 1-y, 1-z$.

Table 3. Selected bond lengths [Å], angles [°], and torsion angles [°] for the crystal structure of **20**. Symmetry operation: $1-x, 1-y, 1-z$.

Ir1–P1	2.2846(4)	Cp(cg)-Ir1-Ir1a	154.43(2)
Ir1–P1a	2.2890(3)	Cp(cg)-Ir1-P1	139.27(2)
Ir1–C9a	2.1330(13)	Cp(cg)-Ir1-P1a	132.80(2)
Ir1–Cp(cg)	1.8793(7)	Cp(cg)-Ir1-C9a	124.88(4)
P1–C1	1.8178(13)	P1-C1-C6	110.93(9)
C1–C6	1.4070(19)	C1-C6-C9	117.17(12)
C6–C9	1.5070(19)	C6-C9-Ir1a	110.01(8)
		C1-P1-Ir1	119.20(4)
C1-C6-C9-Ir1a	−41.16(14)	C1-P1-Ir1a	100.76(4)
P1-C1-C6-C9	6.93(15)	P1-Ir1-C9a	85.83(4)
P1-Ir1-P1a-Ir1a	0	P1-Ir1-P1a	74.370(15)
		Ir1-P1-Ir1a	105.629(15)

The Ir–P distances of 2.2846(4) and 2.2890(3) Å are normal for Ir–P single bonds.[21] The iridium centers have a three-legged piano stool geometry with an acute P1-Ir1-P1a angle of 74.370(15)°. The Ir1–C9a bond length of 2.1330(13) Å is in the normal range for Ir–C bonds in five-membered IrC_4 metallacycles (2.11–2.15 Å).[22]

The strong base BTPP causes double HCl elimination from **18**, but dimer **19**, just as **16**, could not be detected during the reaction, and its subsequent conversion is more speculative. If it is presumed that the iridium centers of the $[IrP]_2$ ring in **19** are reactive, an agostic interaction with a Mes methyl group may induce C–H insertion and hydrogen transfer to the neighbouring phosphorus atom. Carbon–hydrogen activation followed by P-insertion, as in **16**→**17**, would give a strained CCCP ring. After hydrogen transfer, the change in hybridization of the phosphorus atom ($sp^2 \rightarrow sp^3$) may lead to an even better alignment of the other reactive iridium with the remaining Mes substituent to enable a second C–H insertion to occur to give **20**.

There is precedence for the formation of structures similar to **17** and **20**. For example, in the absence of stabilizing ligands ruthenium complex [(η^6-C_6H_6)Ru=PMes*] converges to dimer **21**,[23] while uncomplexed transient Mes*P undergoes intramolecular C–H insertion to afford phosphaindane **22**.[24] Tilley et al.[25] isolated rhodium–phosphaindane complex **23** from the reaction of [Rh(η^3-benzyl)(dippe)] (dippe = 1,2-bis(diisopropylphosphino)-ethane) with Mes^*PH_2. Similarities also arise with zirconocene analogue [Cp_2Zr=PAr]. In the absence of stabilizing ligands, when Ar = Mes* dimers are not formed.[6a] However, transient [{Cp_2Zr=PMes}$_2$] results in the presence of the smaller Mes substituent, and is followed by an intramolecular C–H bond activation of a Cp ligand to give **24**.[26] In the presence of the bigger Cp* ligand, [Cp^*_2Zr=PMes] does not dimerize, but instead undergoes intramolecular insertion into an *o*-Me group to give **25**, which is a monomeric Zr analogue of **20**.[27] Still, stable dimers remain rare. An exception was reported only recently by Hey-Hawkins et al.,[28] who prepared and reported X-ray crystal structures for dimeric tantalum complexes [{Cp*(Cl)Ta=PR}$_2$] (**26**).

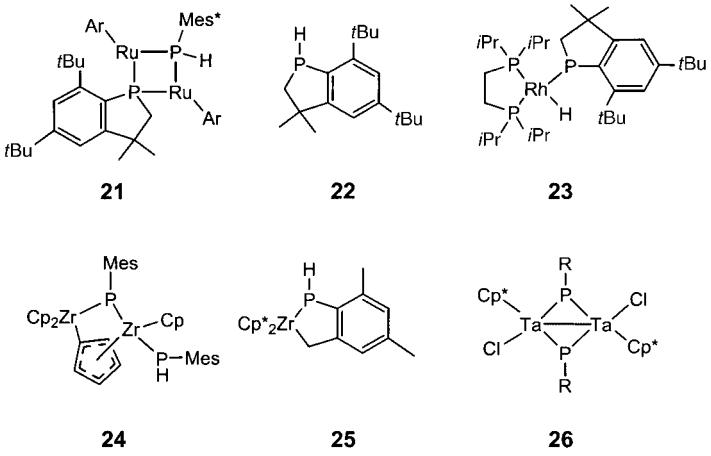

21 **22** **23**

24 **25** **26**

Theoretical evaluation of the [{IrP}$_2$] dimers: The question arises as to why dimers **16** and **19** are unstable. After all, formation of [{CpIrPH}$_2$] (**11**) from the monomer is an exothermic process (-96.4 kcal mol^{-1}). We wondered whether steric effects would enhance the reactivity of **11** by forcing the $[IrP]_2$ ring into a planar disposition that would require only 19.5 kcal mol^{-1} (B3LYP, 12.5 BP86) to change. To study any steric effects, we decided to conduct calculations on the fully

substituted dimer [{Cp*Ir=PMes*}$_2$] (**27**) using the ONIOM methodology, and in particular B3LYP/SDD to optimize the [{CpIr=P}$_2$] geometry and HF/LANL1MB for both the Mes* substituents and the Me groups on the Cp rings (see Computational Section for details). Remarkably, structure **27** (C_i) (Figure 9, Table 4) is only 34.7 kcal mol^{-1} more stable than its monomer, and reflects a large reduction from the dimerization energy of [CpIr=PH].[29] Moreover, its geometry has some resemblance to the crystal structure of **17** (Figure 6). Not only is the structure planar, but the Mes* substituents are bent towards the iridium atoms ($\sphericalangle C_b$–P–Ir 116.3° instead of $\sphericalangle$H–P–Ir 124.2° as in **11′** (C_1)) with each iridium and phosphorus atom being in close contact with a methyl C–H bond (Ir–H 3.155 Å, P–C 3.437 Å). The P–C distance is slightly less than the sum of the van der Waals radii. Likewise, the Ir–H distance represents a borderline agostic interaction. The tight packing of the methyl groups in the Cp* ligands and Mes* substituents illustrates the significant strain in **27**; this is also evident from the way in which the Mes* group tilts and the [IrP]$_2$ ring shows in-plane distortion (Figure 9, Table 4). The Ir–P bond differs by as much as 0.209 Å in relation to the Ir–P′ bond and is rather elongated (2.467 Å, c.f. **11′** $\Delta d = 0.027$ Å).

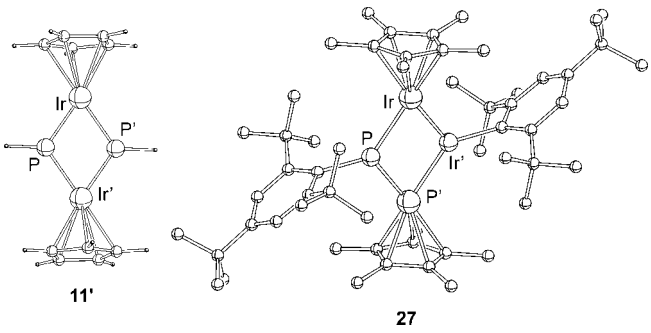

Figure 9. Optimized geometries for [{Cp*IrPMes*}$_2$] (**27**; hydrogens omitted for clarity) and [{CpIrPH}$_2$] (planar, **11′**).

Table 4. Calculated bond lengths [Å], angles [°], and torsion angles [°] for **27** (C_i) and planar **11′** (C_1).

	[{Cp*IrPMes*}$_2$] (**27**)[a]	[{CpIrPH}$_2$] (**11′**)[b]
Ir–P	2.258	2.212
Ir–P′	2.467	2.239
Ir–Ir′	3.813	3.654
Cp–Ir	1.974	2.003
Ir-P-Ir′	107.5	110.4
P-Ir-P′	72.5	69.6
Ir-P-P′-Ir′	180.0	180.0

[a] ONIOM(B3LYP/SDD:HF/LANL1MB). [b] B3LYP/6-31G^{++} and LANL2DZ for Ir.

Clearly, the large substituents have a profound impact on the properties of the [{IrP}$_2$] dimer. The close Ir–H and P–C interactions in **27** are particularly relevant. Formal carbon–hydrogen insertion followed by hydrogen transfer to Ir and P–C bond formation gives the 21.4 kcal mol^{-1} more stable **28** (Figure 10). Structure **28** displayed a structure with features similar to the crystal structure of **17** even though proper comparisons could not be made because of the disorder found in the crystal. The calculated activation barrier of 40.8 kcal mol^{-1} for the rearrangement of **27** is disproportionately high, and is the result of an imbalance in the ONIOM geometry optimization of TS1 in which hydrogen bridging and C–P bond formation occurs between the HF and B3LYP layers (see Computational Section). Further rearrangements are also feasible. In fact, structure **29**, in which the Ir hydride is rotated by ~180°, is 14.2 kcal mol^{-1} more stable than **28**, and has an activation barrier for rearrangement of only 34.9 kcal mol^{-1}. Unfortunately, we were unable to establish the direct conversion of **27** into **29**. The other rearrangement, which would involve the other Mes* substituent and afford **30** from **29** (and subsequently **31**) has a much higher activation barrier of 54.5 kcal mol^{-1} (and 36.4 kcal mol^{-1}) despite being an overall exothermic reaction (−9.3 and −23.1 kcal mol^{-1}, respectively). This process is not observed experimentally for **17**.

Conclusion

The generation, properties, and reactivity of the elusive phosphinidene complex [Cp*Ir=PAr] (**2**) were studied. DFT calculations reveal significant differences in chemical behaviour between model complex [CpIr=PH] (**6**) and its imido analogue **4**. [CpIr=PH] has a bent 16-electron structure **6** with a small inversion barrier, whereas imido analogue **4** strongly prefers a linear 18-electron geometry. The bent structure of [CpIr=PH] facilitates barrierless and energetically highly favorable ligand addition to the electron-deficient iridium center, and leads to bent phosphinidene complexes [Cp(L)Ir=PH] (L = PH_3, CO). Ligand additions to [CpIr≡NH] also exhibit small barriers but are much less exothermic. Dimerizations that lead to puckered bis(phosphinidene) **11** and bis(imido) **12** complexes are highly favorable.

Whereas dimeric imido complexes [{Cp*Ir=NAr}$_2$] are experimentally stable compounds when appropriately substituted, the phosphinidene analogues [{Cp*Ir=PAr}$_2$] could not be isolated. In the absence of ligands and at low temperatures, generation of [Cp*Ir=PAr] renders dimeric structures in which a single (Ar = Mes*) or double (Ar = Mes) insertion has taken place to give fused-ring systems **17** and **20**, respectively. ONIOM calculations conducted on substituted complexes indicate that steric congestion inflicts a less stable planar structure **27**, which can undergo an intramolecular insertion to give **28**.

Computational Section

The DFT calculations were performed with the parallelized Amsterdam Density Functional package (ADF version 2002.01).[30] All atoms were described by a triple-ζ basis set with polarization functions and frozen cores for the carbon 1s and phosphorus 1s2s2p shells. For iridium, a triple-ζ basis set was used for the outer *n*s, *n*p, *n*d, and (n + 1s) orbitals. All calculations were performed self-consistently at the non-local BP86 level using the local density approximation (LDA) in the Vosko–Wilk–Nusair parametization,[31] and non-local corrections for exchange

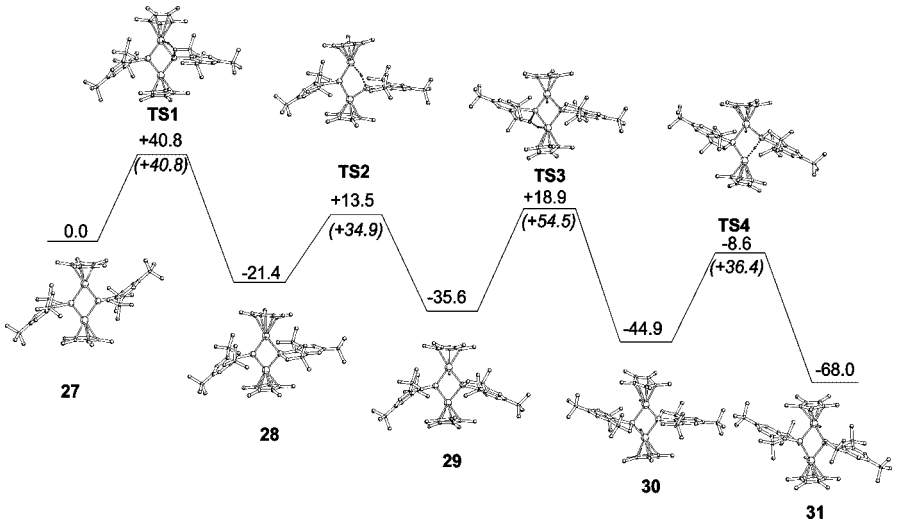

Figure 10. B3LYP/SDD//ONIOM(B3LYP/SDD:HF/LANL1MB energy profile (in kcal mol^{-1}) for the rearrangement of [{Cp*IrPMes*}$_2$] (**27**). Only the IrH hydrogen atom is depicted for clarity.

(Becke88)[32] and correlation (Perdew86).[33] Geometries were optimized,[34,35] with relativistic effects included, by the zero-order regular approximation (ZORA).[36] Transition state structures were verified to have only one imaginary frequency.[37] Atomic charges were calculated according to the definition of Hirshfeld.[38] The Ir=P and Ir=N bonds were analyzed with ADF's energy decomposition[39] into an exchange repulsion and electrostatic interaction energy part ($\Delta E°$), an orbital interaction energy (charge transfer, polarization) part (ΔE^{oi}), and a preparation energy term (ΔE^{prep}) in order to convert fragments from their ground state equilibrium geometries to those they acquire in the complex. The overall bond energy (ΔE^{tot}) was formulated as $\Delta E^{tot} = \Delta E° + \Delta E^{oi} + \Delta E^{prep}$, and defined as the negative of the bond dissociation energy (BDE, $\Delta E^{tot} = E(\text{molecule}) - \Sigma E(\text{fragments})$). The orbital interaction term ΔE^{oi} accounts for charge transfer (interactions between occupied orbitals on one fragment with unoccupied orbitals on the other, including HOMO–LUMO interactions) and polarization (empty/occupied orbital mixing on the same fragment). The charge transfer part is the result of both σ donation from the ligand to the metal and π back-donation from the metal into the unoccupied orbitals of the ligand. We used the extended transition state (ETS) method to decompose ΔE^{oi} into contributions from irreducible representations; this is the most informative for systems with a clear σ, π separation.[40] The Gaussian 98 suite of programs (G98 Revision A.11.1)[41] in which the Becke's hybrid three-parameter functional[32] was combined with the Lee–Yang–Parr correlation functional,[41] denoted as B3LYP, was used to optimize the geometries for compounds **28** and **29**. The Los Alamos National Laboratory basis set for effective core potentials (ECP) of double ζ type (LANL2DZ) was used for iridium; this includes relativistic effects and 6-31G^{++} for the other elements. Two-layer ONIOM calculations were employed for the large systems **27**, **30**–**33**, and transition structures **TS1**–**TS4**. Geometries were optimized using B3LYP and the SDD basis set with effective core potentials for their central component **27**, while Hartree–Fock (HF) and the LANL1MB basis set was used for the other atoms. Single-point energy calculations were then performed at the B3LYP/SDD level using the 6-311G+ basis set for phosphorus.

Experimental Section

All experiments were performed in flame-dried glassware under an atmosphere of dry nitrogen or argon. Those on a small scale were performed in Wilmad Ultra-Imperial screw-cap NMR tubes (Aldrich). Solvents were distilled (under N_2) from sodium (toluene) and diphosphorus-pentoxide (CH_2Cl_2). Deuterated solvents were dried over 4 Å molecular sieves (CD_2Cl_2, [D_8]toluene). All solid starting materials were dried under vacuum. ^{1}H, ^{13}C, and ^{31}P NMR spectra were recorded on a Bruker Avance 250 spectrometer at 250.13, 62.90, and 101.25 MHz, respectively, while low-temperature ^{1}H and ^{31}P NMR spectra were recorded on a Bruker Avance 400 spectrometer at 400.13 and 162.06 MHz, respectively. ^{1}H NMR spectra were referenced to $CHDCl_2$ ($\delta = 5.30$ ppm) or C_7D_7H ($\delta = 2.09$ ppm), ^{13}C NMR spectra were referenced to C_7D_8 ($\delta = 20.4$ ppm), while ^{31}P NMR spectra were referenced to external 85 % H_3PO_4. IR spectra were recorded on a Mattson-6030 Galaxy FTIR spectrophotometer. Elemental analyses were performed by Mikroanalytisches Labor Pascher, Remagen-Bandorf, Germany. [Cp*IrCl$_2$(PH$_2$Mes*)] and [Cp*IrCl$_2$(PH$_2$Mes)] were prepared according to literature procedures.[8] BTPP was purchased from Fluka and was used as received.

Dehydrohalogenation of 1a at room temperature: BTPP (30.6 μL, 0.100 mmol) was added to an orange solution of **1a** (33.8 mg, 0.050 mmol) in CD_2Cl_2 (0.6 mL) in a screw-capped NMR tube at room temperature. The resultant deep purple solution was monitored by ^{31}P NMR spectroscopy to show the formation of **13** (92 %). ^{31}P NMR (101.25 MHz, CD_2Cl_2, 300 K): $\delta = 699$ (d, $^2J_{P,P} = 20$ Hz, Ir=P), −85.3 ppm (dt, $^1J_{P,H} = 384$ and $^2J_{P,P} = 20$ Hz, IrPH$_2$).

Dehydrohalogenation of 1a at low temperature: The same reaction was executed at −70 °C using **1a** (33.8 mg, 0.050 mmol) and 1.5 equivalents of BTPP (23.0 μL, 0.075 mmol). The major product was identified as **15**. ^{31}P NMR (162.06 MHz, CD_2Cl_2, 203 K): $\delta = 386.8$ (dd, $^2J_{P,P} = 43$ and $^3J_{P,H} = 35$ Hz), −125.4 ppm (dd, $^1J_{P,H} = 446$ and $^3J_{P,P} = 43$ Hz); ^{1}H NMR (400.13 MHz, CD_2Cl_2, 203 K): $\delta = 6.36$ (dd, $^1J_{P,H} = 446$ and $^3J_{P,H} = 35$ Hz), 7.36 (s, 1H; *m*-Mes*), 7.46 (s, 1H; *m*-Mes*), 7.51 ppm (s, 2H; *m*-Mes*).

Upon warming the solution to −20 °C, a second unidentified product was formed. ^{31}P NMR (162.06 MHz, CD_2Cl_2, 253 K): $\delta = 285$ (d, $J_{P,H} = 26$ Hz); ^{1}H NMR (400.13 MHz, CD_2Cl_2, 253 K): $\delta = -6.70$ (t, $J_{P,H} = 26$ Hz, IrH), 7.30 (s, 1H; *m*-Mes*), 7.33 (s, 1H; *m*-Mes*).

The ^{1}H NMR resonances for the *tert*-butyl and Cp* groups in either of the two cases above could not be fully assigned because of the presence of BTPP. Upon further addition of BTPP (7.7 μL, 0.025 mmol) and subsequent warming to room temperature all resonances disappeared, except for those of BTPP·HCl and a solid that precipitated from the reaction mixture, which was identified as **17**. Upon repeating the same reaction at −70 °C using **1a** (271 mg, 0.40 mmol) in CH_2Cl_2 (5 mL) and 2.2 equivalents of BTPP (275 μL, 0.90 mmol), but with slow warming to room temperature, air-sensitive red crystals of **17** (191 mg, 79 %) were isolated, m.p. >320 °C (decomp). ^{31}P NMR (101.25 MHz, CD_2Cl_2, 323 K): $\delta = 183.6$ (dd, $^2J_{P,P} = 198$ and $^2J_{P,H} = 34$ Hz, phosphinidene), −176.7 ppm (dd, $^2J_{P,P} = 198$ and $^2J_{P,H} = 25$ Hz, phosphindole); ^{1}H NMR (250.13 MHz, CD_2Cl_2, 323 K): $\delta = -14.80$ (dd, $^2J_{P,H} = 34$ and 25 Hz, 1H; IrH), 1.33 (s, 3H; CH_3), 1.39 (s, 18H; *o*-C(CH$_3$)$_3$), 1.41 (s, 9H; C(CH$_3$)$_3$), 1.44 (s, 15H; C$_5$(CH$_3$)$_5$), 1.45 (s, 15H; C$_5$(CH$_3$)$_5$), 1.74 (s, 3H; CH_3), 1.85 (s, 9H; C(CH$_3$)$_3$), 1.86 (s, 9H; C(CH$_3$)$_3$), 3.25 (dd, $^2J_{H,H} = 14$ and $^4J_{P,H} = 4.5$ Hz, 1H; CH_2), 3.47 (dd, $^2J_{H,H} = 14$ and $^4J_{P,H} = 7.8$ Hz, 1H; CH_2), 7.13 (d, $^4J_{H,H} = 2.0$ Hz, 1H; ArH), 7.37 (s, 2H; ArH), 7.41 ppm (d, $^4J_{H,H} = 2.1$ Hz, 1H; ArH); ^{13}C NMR data could not be obtained because of the low solubility of **17**; elemental analysis calcd (%) for $C_{56}H_{88}P_2Ir_2$: C 55.69, H 7.35, P 5.13; found: C 55.01, H 7.16, P 5.04.

Dehydrohalogenation of 1b: The same small-scale reaction was performed at −80 °C using **1b** (27.5 mg, 0.050 mmol) and 1 equivalent of BTPP (15.3 μL, 0.050 mmol) to give **18** as a 1:2:10 mixture of two symmetrical and one asymmetrical isomers as identified by their ^{31}P NMR resonances at $\delta = -208$ ($^1J_{P,H} = 359$ Hz), −189 ($^1J_{P,H} = 354$ Hz), −147

($^1J_{P,H}=351$ and $^2J_{P,P}=166$ Hz), and −202 ppm ($^1J_{P,H}=367$ and $^2J_{P,P}=166$ Hz). Addition of a further equivalent of BTPP followed by warming of the reaction mixture to room temperature, and (after 3d) isolation and crystallization (toluene) of the resultant precipitate afforded **20** (16.2 mg, 68%), m.p. >310°C (decomp). ^{31}P NMR (101.25 MHz, [D$_8$]toluene, 343 K): $\delta=-169.6$ ppm (m, $^1J_{P,H}=308$ Hz); ^{1}H NMR (250.13 MHz, [D$_8$]toluene, 343 K): $\delta=1.48$ (t, $^4J_{P,H}=2.0$ Hz, 30H; $C_5(CH_3)_5$), 2.07 (m, $^1J_{P,H}=308$ Hz, 2H; PH), 2.20 (s, 6H; CH_3), 2.31 (s, 6H; CH_3), 2.99 (m, $^2J_{H,H}=13.8$ Hz, 2H; CH_2), 3.59 (m, $^2J_{H,H}=13.8$ Hz, 2H; CH_2), 6.49 (s, 2H; ArH), 6.99 ppm (s, 2H; ArH); ^{13}C{^{1}H} NMR (62.90 MHz, [D$_8$]toluene, 343 K): $\delta=8.8$ (s, $C_5(CH_3)_5$), 8.5 (s, CH_2), 21.1 (s, CH_3), 21.3 (s, CH_3), 91.8 (s, $C_5(CH_3)_5$), 125.3 (s, HCMes), 125.6 (s, HCMes), 135.2 (s, CH_2CMes), 136.9 (s, CH_3CMes), 136.9 (d, $^3J_{PC}=1.2$ Hz, CH_3CMes), 159.9 (d, $^1J_{PC}=30$ Hz, PCMes); IR (KBr): $\tilde{\nu}=2226$ cm^{-1} (PH).

Crystal structure determination of complexes 17 and 20: X-ray intensities were measured on a Nonius KappaCCD diffractometer with a rotating anode and Mo$_{K\alpha}$ radiation (graphite monochromator, $\lambda=0.71073$ Å). An analytical absorption correction was applied using the program PLATON.[42] The reflections were merged using the program SORTAV.[43] The structures were solved with automated Patterson methods using the program DIRDIF,[44] and were refined with the program SHELXL97[45] against F^2 of all the reflections. The structure of **17** was disordered over an inversion center and the interpretation of the electron density was based on NMR spectra (see text). One disorder component contains the phosphinidene ligand, while the other disorder component contains iridium hydride and the cyclic phosphide ligand. The position of the hydride could not be determined experimentally. In the structure of **20**, the P–H hydrogen atom was located in the difference Fourier map and kept fixed in that position. The drawings, structure calculations, and checking for higher symmetry was performed with the program PLATON.[42] Further crystallographic details are given in Table 5.

CCDC-229359 (**17**) and CCDC-229360 (**20**) contain the supplementary crystallographic data for this paper. These data can be obtained free of charge via www.ccdc.cam.ac.uk/conts/retrieving.html (or from the CCDC, 12 Union Road, Cambridge CB2 1EZ, UK; fax: (+44) 1223-336033; or e-mail: deposit@ccdc.cam.ac.uk).

Table 5. Crystallographic details for **17** and **20**.

	Compound **17**	Compound **20**
empirical formula	$C_{56}H_{88}Ir_2P_2$	$C_{38}H_{52}Ir_2P_2$
formula weight	1207.60	955.14
temperature [K]	110(2)	110(2)
crystal system	monoclinic	triclinic
space group	$P2_1/c$ (no. 14)	$P\bar{1}$ (no. 2)
a [Å]	12.7661(7)	8.2839(3)
b [Å]	16.8609(5)	10.7846(7)
c [Å]	12.1723(5)	11.2332(9)
α [°]	90	62.010(6)
β [°]	97.698(4)	74.386(5)
γ [°]	90	77.532(4)
V [Å^3]	2596.5(2)	848.72(10)
Z	2	1
ρ_{calcd} [g cm^{-3}]	1.545	1.869
μ [mm^{-1}]	5.216	7.952
F (000)	1216	464
crystal size [mm^3]	0.21×0.15×0.12	0.27×0.15×0.12
$(\sin\theta/\lambda)_{max}$	0.65	0.90
reflections collected	53438	67640
unique reflections	5975	10352
absorption correction	analytical	analytical
transmission range	0.37–0.63	0.19–0.59
no. of parameters	312	190
no. of restraints	53	0
R [$I>2\sigma(I)$]	0.0299	0.0176
R (all data)	0.0342	0.0195
wR_2 (all data)	0.0610	0.0436
goodness-of-fit on F^2	1.119	1.075

Acknowledgements

This work was supported by The Netherlands Foundation for Chemical Sciences (CW) with financial aid from The Netherlands Organization for Scientific Research (NWO).

[1] a) A. H. Cowley, A. R. Barron, *Acc. Chem. Res.* **1988**, *21*, 81–87; b) A. H. Cowley, *Acc. Chem. Res.* **1997**, *30*, 445–451.
[2] a) F. Mathey, N. H. T. Huy, A. Marinetti, *Helv. Chim. Acta* **2001**, *84*, 2938–2957; b) K. Lammertsma, M. J. M. Vlaar, *Eur. J. Org. Chem.* **2002**, 1127–1138.
[3] a) K. B. Dillon, F. Mathey, J. F. Nixon, *Phosphorus: The Carbon Copy*; Wiley: Chichester, **1998**, Chapter 3; b) K. Lammertsma, *Phosphinidenes, in Topics in Current Chemistry: New Aspects in Phosphorus Chemistry III,* (Ed.: J.-P .Majoral), Springer, **2003**.
[4] a) C. C. Cummins, R. R. Schrock, W. M. Davis, *Angew. Chem.* **1993**, *105*, 758–761; b) J. S. Freundlich, R. R. Schrock, W. M. Davis, *J. Am. Chem. Soc.* **1996**, *118*, 3643–3655.
[5] a) A. H. Cowley, B. Pellerin, *J. Am. Chem. Soc.* **1990**, *112*, 6734–6735; b) G. Hogarth, D. G. Humphrey, N. Kaltsoyannis, W.-S. Kim, M. Lee, T. Norman, S. P. Redmond, *J. Chem. Soc. Dalton Trans.* **1999**, 2705–2723.
[6] a) Z. Hou, T. L. Breen, D. W. Stephan, *Organometallics* **1993**, *12*, 3158–3167; b) T. L. Breen, D. W. Stephan, *J. Am. Chem. Soc.* **1995**, *117*, 11914–11921.
[7] a) P. J. Walsh, F. J. Hollander, R. G. Bergman, *J. Am. Chem. Soc.* **1988**, *110*, 8729–8731; b) P. J. Walsh, F. J. Hollander, R. G. Bergman, *Organometallics* **1993**, *12*, 3705–3723.
[8] A. T. Termaten, T. Nijbacker, M. Schakel, M. Lutz, A. L. Spek, K. Lammertsma, *Organometallics* **2002**, *21*, 3196–3202.
[9] A. T. Termaten, H. Aktas, M Schakel, A. W. Ehlers, M. Lutz, A. L. Spek, K. Lammertsma, *Organometallics* **2003**, *22*, 1827–1834.
[10] D. S. Glueck, J. Wu, F. J. Hollander, R. G. Bergman, *J. Am. Chem. Soc.* **1991**, *113*, 2041–2054.
[11] E. W. Jandciu, P. Legzdins, W. S. McNeil, B. O. Patrich, K. M. Smith, *Chem. Commun.* **2000**, 1809–1810.
[12] a) D. W. Rankin, H. E. Robertson, A. A. Danopoulos, P. D. Lyne, D. M. P. Mingos, G. Wilkinson, *J. Chem. Soc. Dalton Trans.* **1994**, 1563–1569; b) K. A. Jørgensen, *Inorg. Chem.* **1993**, *32*, 1521–1522; c) W. A. Nugent, J. M. Mayer, *Metal-Ligand Multiple Bonds*, Wiley: New York, **1989**; d) J. H. Osborne, A. L. Rheingold, W. C. Trogler, *J. Am. Chem. Soc.* **1985**, *107*, 7945–7952; e) T. R. Cundari, *J. Am. Chem. Soc.* **1992**, *114*, 7879–7888.
[13] All the fragments have strongly preferred triplet ground states, 53.7 (NH), 34.6 (PH), and 12.2 kcal mol^{-1} (CpIr) more stable than their closed shell singlet states.
[14] The relative charges concur with the atom electronegativities (χ(N) 3.0; χ(P) 2.1). L. Pauling, *The Nature of the Chemical Bond*, 3rd ed., Cornell University Press, Ithaca, N.Y., **1960**, 88–93.
[15] A. W. Ehlers, E.-J. Baerends, K. Lammertsma, *J. Am. Chem. Soc.* **2002**, *124*, 2831–2838.
[16] An alternative mechanism, which involved [1+2] cycloaddition of CO to the Ir≡N bond to form an isocyanate complex directly, cannot be excluded. Here, we focused on the phosphinidene and imido complexes, and this alternative reaction pathway has not been analyzed further.
[17] a) D. A. Dobbs, R. G. Bergman, *J. Am. Chem. Soc.* **1993**, *115*, 3836–3837; b) D. A. Dobbs, R. G. Bergman, *Organometallics* **1994**, *13*, 4594–4605.
[18] C. White, A. Yates, P. M. Maitlis, *Inorg. Synth.* **1992**, *29*, 228–230.
[19] Compound **17** hardly dissolves in any solvent. Identical IR spectra, recorded before and after heating, indicate that **17** does not decompose at elevated temperatures.
[20] The 2,4,6-triisopropylphenylphosphine complex [Cp*IrCl$_2$(PH$_2$Is)] (**1c**) was also briefly investigated, but dehydrohalogenation at low temperatures led to an unidentifiable mixture of products.
[21] J. Le Bras, H. Amouri, J. Vaissermann, *J. Organomet. Chem.* **1997**, *548*, 305–309.
[22] a) R. Bertani, P. Diversi, G. Ingrosso, A. Lucherini, F. Marchetti, V. Adovasio, M. Nardelli, S. Pucci, *J. Chem. Soc. Dalton Trans.* **1988**,

2983–2994; b) P. Diversi, G. Ingrosso, A. Lucherini, W. Porzio, M. Zocchi, *Inorg. Chem.* **1980**, *19*, 3590–3597.
[23] A. T. Termaten, T. Nijbacker, M. Schakel, M. Lutz, A. L. Spek, K. Lammertsma, *Chem. Eur. J.* **2003**, *9*, 2200–2208.
[24] a) M. Yoshifuji, T. Sato, N. Inamoto, *Chem. Lett.* **1988**, 1735–1738; b) A. H. Cowley, M. Pakulski, *Tetrahedron Lett.* **1984**, *25*, 2125–2126; c) M. Yoshifuji, I. Shima, K. Ando, N. Inamoto, *Tetrahedron Lett.* **1983**, *24*, 933–936; d) A. H. Cowley, J. E. Kilduff, N. C. Norman, M. Pakulski, J. L. Atwood, W. E. Hunter, *J. Am. Chem. Soc.* **1983**, *105*, 4845–4846.
[25] M. Stradiotto, K. L. Fujdala, T. D. Tilley, *Helv. Chim. Acta* **2001**, *84*, 2958–2970.
[26] T. L. Breen, D. W. Stephan, *Organometallics* **1996**, *15*, 4509–4514.
[27] Z. Hou, D. W. Stephan, *J. Am. Chem. Soc.* **1992**, *114*, 10088–10089.
[28] S. Blaurock, E. Hey-Hawkins, *Eur. J. Inorg. Chem.* **2002**, 2975–2984.
[29] The dimerization energy for [CpIr=PH] (**11**) amounts to 86.9 kcal mol^{-1} at B3LYP/6-31G^{++} and LANL2DZ for Ir. The energy difference with planar **11′** amounts to 19.5 kcal mol^{-1} at this level.
[30] a) G. te Velde, F. M. Bickelhaupt, S. J. A. van Gisbergen, C. Fonseca Guerra, E. J. Baerends, J. G. Snijders, T. Ziegler, "Chemistry with ADF", *J. Comput. Chem.* **2001**, *22*, 931–967; b) C. Fonseca Guerra, J. G. Snijders, G. te Velde, E. J. Baerends, *Theor. Chem. Acc.* **1998**, *99*, 391; c) ADF2000.02, SCM, Theoretical Chemistry, Vrije Universiteit, Amsterdam, The Netherlands, http://www.scm.com.
[31] S. H. Vosko, L. Wilk, M. Nusair, *Can. J. Phys.* **1980**, *58*, 1200–1211.
[32] A. D. Becke, *Phys. Rev. A* **1988**, *38*, 3098–3100.
[33] J. P. Perdew, *Phys. Rev. B* **1986**, *33*, 8822–8824.
[34] a) L. Fan, L. Versluis, T. Ziegler, E. J. Baerends, W. Raveneck, *Int. J. Quantum Chem. Quantum Chem. Symp.* **1988**, *22*, 173–181.
[35] a) L. Versluis, T. Ziegler, *J. Chem. Phys.* **1988**, *88*, 322–328; b) L. Fan, T. Ziegler, *J. Am. Chem. Soc.* **1992**, *114*, 10890–10897.
[36] E. van Lenthe, A. W. Ehlers, E. J. Baerends, *J. Chem. Phys.* **1999**, *110*, 8943–8953.
[37] a) A. Berces, T. Ziegler, L. Fan, *J. Phys. Chem.* **1994**, *98*, 1584–1595; b) L. Fan, T. Ziegler, *J. Phys. Chem.* **1992**, *96*, 6937–6941.
[38] a) F. L. Hirshfeld, *Theor. Chim. Acta* **1977**, *44*, 129–138; b) K. B. Wiberg, P. R. Rablen, *J. Comput. Chem.* **1993**, *14*, 1504–1518.
[39] a) K. Morokuma, *Acc. Chem. Res.* **1977**, *10*, 294–300; b) T. Ziegler, A. Rauk, *Inorg. Chem.* **1979**, *18*, 1755–1759; c) T. Ziegler, A. Rauk, *Theor. Chim. Acta* **1977**, *46*, 1–10.
[40] M. J. Frisch, G. W. Trucks, H. B. Schlegel, G. E. Scuseria, M. A. Robb, J. R. Cheeseman, V. G. Zakrzewski, J. A. Montgomery, Jr., R. E. Stratmann, J. C. Burant, S. Dapprich, J. M. Millam, A. D. Daniels, K. N. Kudin, M. C. Strain, O. Farkas, J. Tomasi, V. Barone, M. Cossi, R. Cammi, B. Mennucci, C. Pomelli, C. Adamo, S. Clifford, J. Ochterski, G. A. Petersson, P. Y. Ayala, Q. Cui, K. Morokuma, D. K. Malick, A. D. Rabuck, K. Raghavachari, J. B. Foresman, J. Cioslowski, J. V. Ortiz, A. G. Baboul, B. B. Stefanov, G. Liu, A. Liashenko, P. Piskorz, I. Komaromi, R. Gomperts, R. L. Martin, D. J. Fox, T. Keith, M. A. Al-Laham, C. Y. Peng, A. Nanayakkara, C. Gonzalez, M. Challacombe, P. M. W. Gill, B. Johnson, W. Chen, M. W. Wong, J. L. Andres, C. Gonzalez, M. Head-Gordon, E. S. Replogle, and J. A. Pople, *Gaussian 98*, Revision A.7, Gaussian Inc., Pittsburgh PA, **1998**.
[41] C. Lee, W. Yang, R. G. Parr, *Phys. Rev. B* **1988**, *37*, 785–789.
[42] A. L. Spek, *J. Appl. Crystallogr.* **2003**, *36*, 7–13.
[43] R. H. Blessing, *J. Appl. Crystallogr.* **1997**, *30*, 421–426.
[44] P. T. Beurskens, G. Admiraal, G. Beurskens, W. P. Bosman, S. Garcia-Granda, R. O. Gould, J. M. M. Smits, C. Smykalla, The DIRDIF99 program system, Technical Report of the Crystallography Laboratory, University of Nijmegen (The Netherlands), **1999**.
[45] G. M. Sheldrick, SHELXL-97, Program for crystal structure refinement. University of Göttingen (Germany), **1997**.

Received: January 23, 2004
Published online: July 5, 2004

